Supporting Information for:

An Ultra-Clean Tip-Wear Reduction Scheme for Ultrahigh Density Scanning Probe-based Data Storage

Noureddine Tayebi,[1,2] Yuegang Zhang[1, 3, *], Robert J. Chen[1], Quan Tran[1], Rong Chen[1], Yoshio Nishi[2], Qing Ma[1] and Valluri Rao[1]

[1] Intel Corporation, 2200 Mission College Boulevard, Santa Clara, California 95054, USA.

[2] Department of Electrical Engineering, Stanford University, 420 Via Palou Mall, Stanford, California 94305, USA.

[3] The Molecular Foundry, Lawrence Berkeley National Laboratory, Berkeley, California 94720, USA.

* Corresponding author: yzhang5@lbl.gov

Ultra-high density writing. The ultra-high density (3.6 Tbit/inch^2 storage density over 1×1 μm^2) writing shown in Figure 1c in the main manuscript is achieved following two steps. First, the ideal pulse width and voltage to write bits at the size required for the desired density are determined. These conditions are obtained by writing a 19×19 matrix of inverted domains whose columns are written with varying voltage from 7 down to 3.5 V, and whose rows with varying pulse width from 500 ns up to 5 μs, as shown in Figure S1a. The optimum voltage was 4.4 V with a 500 ns with which 8 nm bits were reliably written. Second, the checkerboard pattern is written at the desired density using the voltage and pulse width conditions determined in the first step. The checkerboard high density writing is achieved by writing bits only during the trace scan of the probe-tip over the film. This is depicted in the schematic of Figure S1b. The ultrahigh density writing scheme which utilizes a dual CMOS scheme is shown in Figure S2.

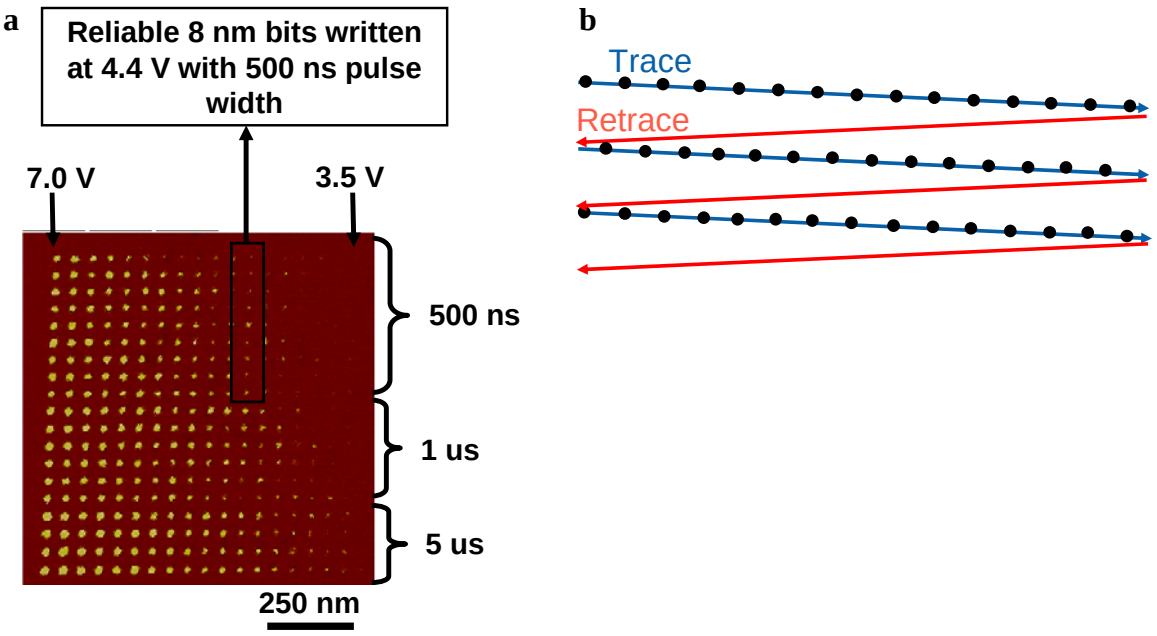

Figure S1. Ultra-high density writing procedure. (a) 19×19 matrix of inverted domains with columns written with varying voltage from 7 down to 3.5 V and rows with varying time pulse from 500 ns up to 5 μs. Ideal conditions for reliable 8 nm bit writing are achieved at 4.4 V with 500 ns pulse width. (b) Checkerboard writing scheme using ideal conditions determined in (a).

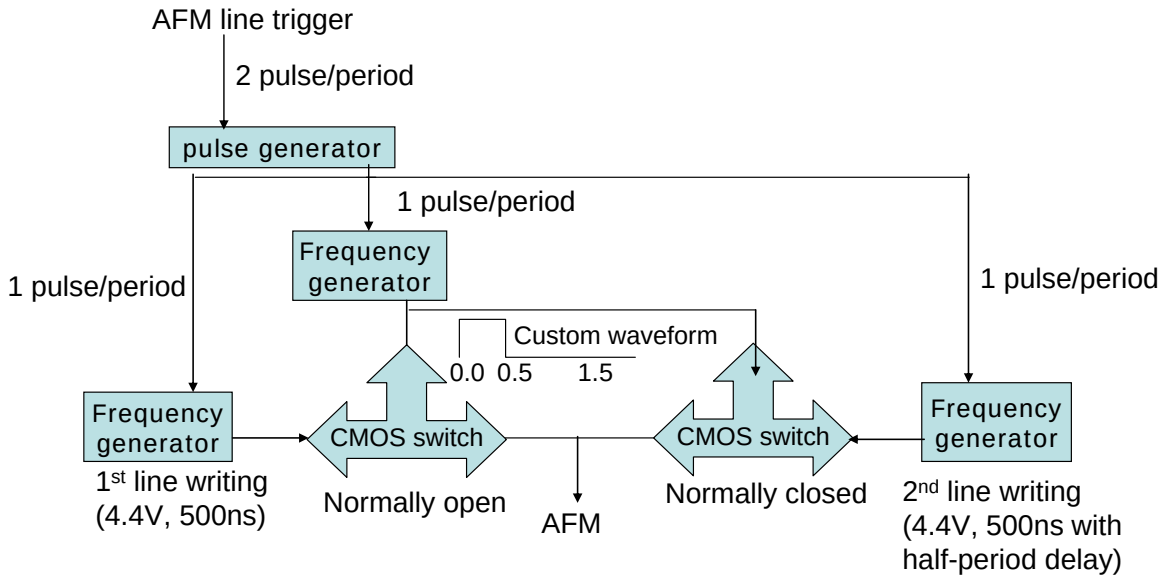

Figure S2. Diagram of ultrahigh density writing scheme using dual CMOS switching.

Electrical hot spots. The defects in the recording shown in Figure1c are due to electrical hot spots originating from defects in the ferroelectric film. The resistance in these regions is in the range of 590 kΩ - 120 MΩ. In these regions, the electric field is smaller than other regions where recording was obtained, which causes bits not be written. These hot spots correspond to dead spots during the PFM readout as shown in Figure S3, which compares resistance mapping with PFM phase mapping of the ferroelectric film over the same scanning area.

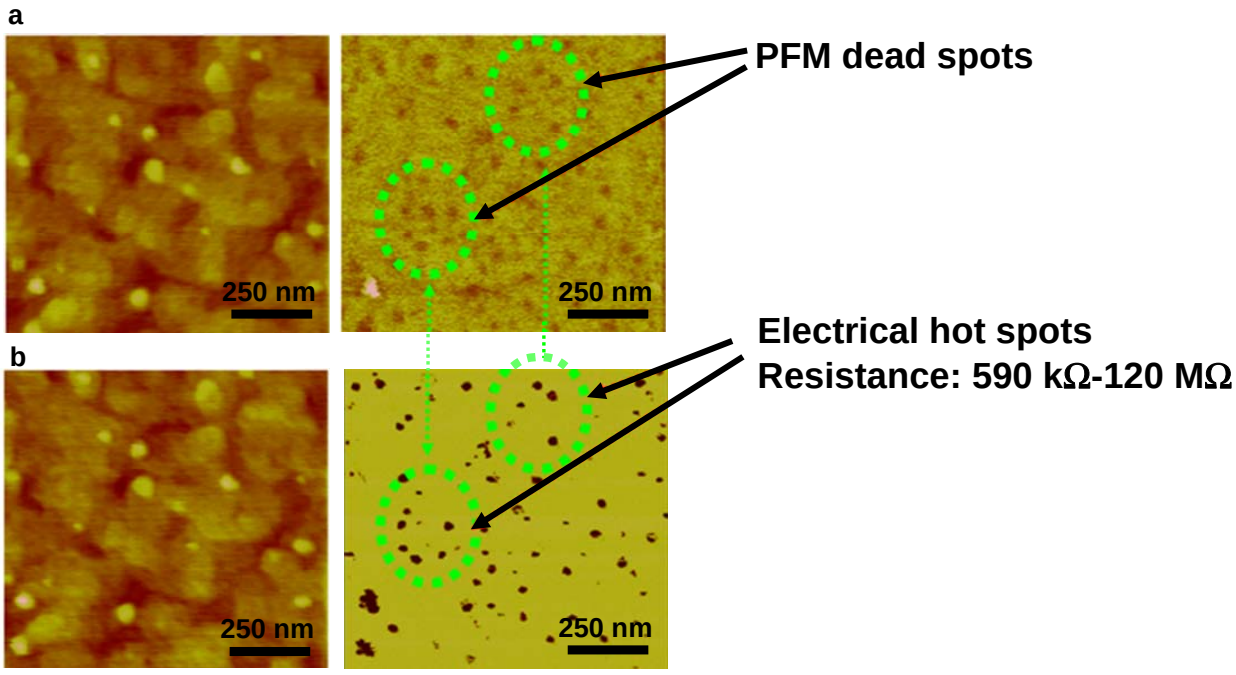

Figure S3. Electrical hot spots in ferroelectric film. (a) Height and PFM phase images where dead spots are highlighted. (b) Height (same region as in (a)) and resistance mapping images showing electrical hot spots corresponding to the PFM dead spots shown in (a). The PFM mapping is obtained at 0 V dc bias with a 0.25 V ac bias at 66 kHz frequency, whereas the resistance mapping is obtained at 3 V dc bias with a 0.25 V ac at 66 kHz frequency.

Adhesion pull-off force determination under 25% RH. The adhesion pull-off force is measured from force-displacement measurements as the probe-tip is brought into contact with the sample and then withdrawn (Figure S4). The steps in obtaining such measurements are as follows. First, the tip is moved towards the surface (red trace). A jump in the deflection is seen, which is a measure of the attractive forces between the tip and the sample surface, reaching a critical value, upon which the tip touches the sample (point A on the red trace in Figure S4). This critical value corresponds to the pull-on point. When the deflection reaches a set-point, the tip starts to retract from the surface (blue trace). However, due to the presence of adhesion forces, the tip remains in contact until a critical deflection is reached, which exceeds the adhesive interaction between the tip and the sample surface. This critical deflection corresponds to the pull-off point (point B in Figure S4). Note that Figure S4 shows the variation of the cantilever deflection as function of the normal approach. The actual pull-off force is calculated by multiplying the critical pull-off deflection by the cantilever vertical stiffness, which in the current study is measured to be 296.93 pN/nm. This corresponds to a pull-off force of 17.82 nN ≅ 18 nN. The adhesion pull-off force can also be estimated from the $2\pi\gamma R$ adhesion term in the DMT adhesion model. Using the adhesion energy of water γ = 140 mN/m and tip radius R = 20 nm, the pull-off force is estimated to be 17.59 nN which is in very good agreement with the experimental value.

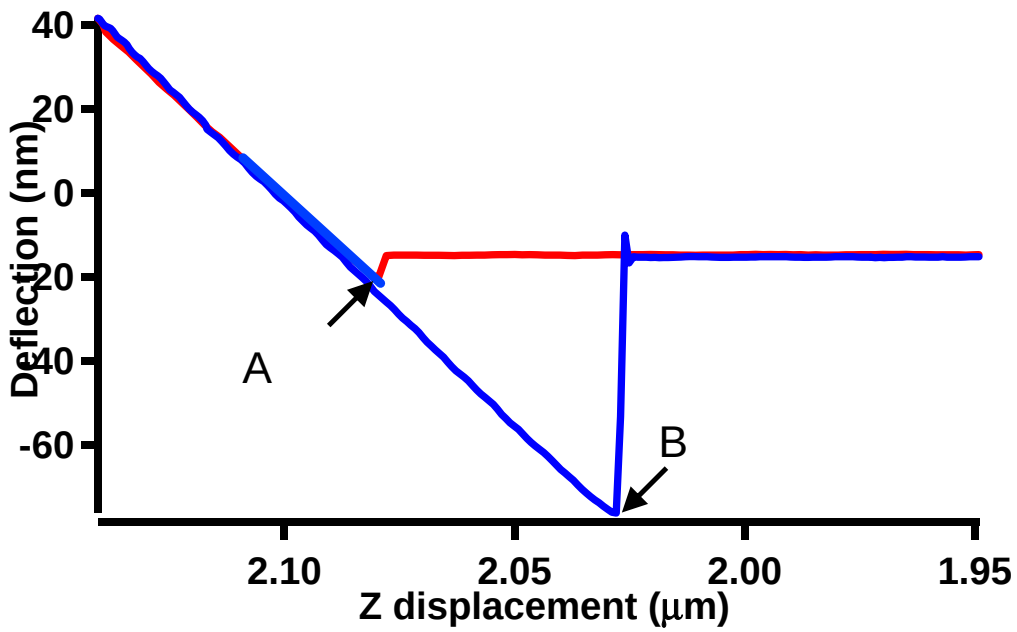

Figure S4. AFM pull-off force measurement for the contact between PtIr probe-tip and PZT surface.

Determination of wear volume. Wear volumes after sliding were determined by comparing SEM images of probe-tips before and after sliding. Figure S5a depicts an as-received probe-tip overlapped on the tip after 2.5 km sliding (Figure 3b). The amount of wear volume is highlighted. In this case it is a spherical cap whose volume is given by $V = \frac{\pi}{6}\left(3r_b^2 + h^2\right)h$ where r_b is the base radius and h is the cap height (see Figure S5b). To determine the wear volume after the 5 km, the probe-tip after 2.5 km sliding is overlapped on the probe-tip after 5 km (Figure S5c). This value is added to the wear volume after 2.5 km sliding. Note that there is an error associated with SEM resolution which we estimate to be ± 3 nm. The error bars in Figure 4 correspond to this resolution error.

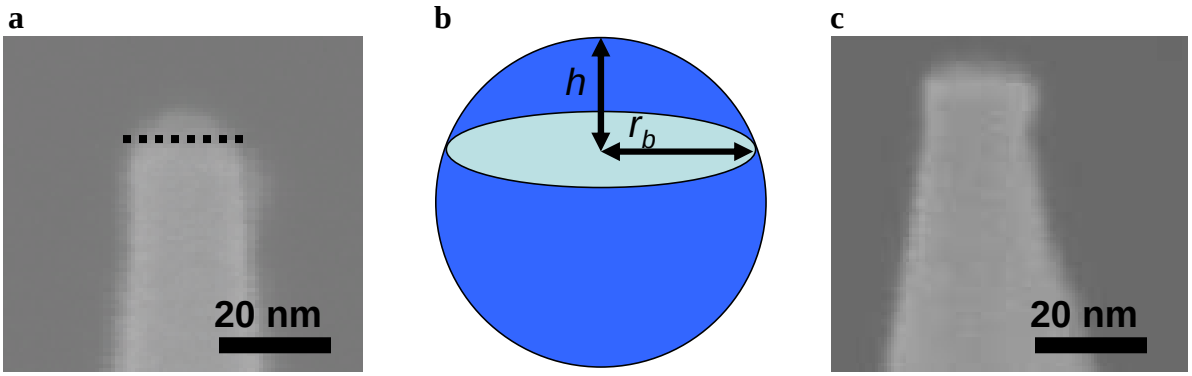

Figure S5. Tip-wear volume determination. (a) As received tip overlapped on the worn tip after 2.5 km sliding corresponding to Figure 3b. (b) schematic of a spherical cap used to estimate wear volume. (c) Worn probe-tip after 2.5 km sliding is overlapped on the probe-tip after 5 km to determine the total wear volume after 5 km sliding corresponding to Figure 3c.

Domain size determination. Domain size is determined by inspecting line scans of the inverted domains. Figures S6a,b show line scans taken over inverted domains shown in Figures 3d,e where inverted domain sizes of 15.6 nm are determined.

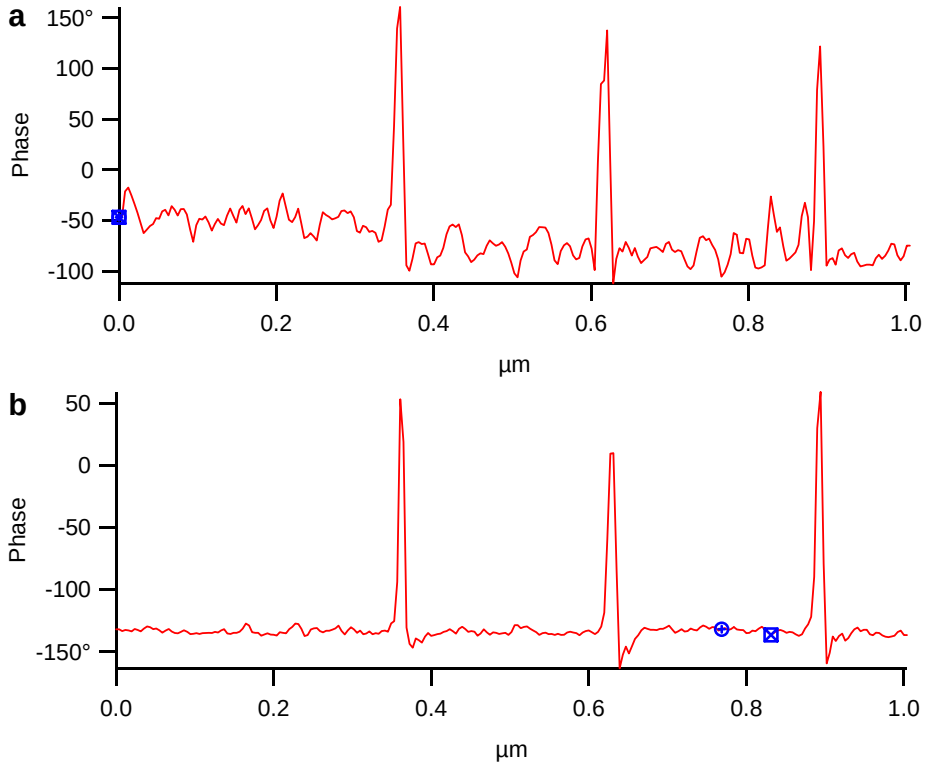

Figure S6. Scan profiles of inverted domains before (a) and after (b) 5 km sliding (Figure 3).

Effect of probe-shape on write-read resolution. When writing on ferroelectric media, there are various parameters that determine the bit size. While the tip size and shape are the main ones, there are other parameters that are as important and which are solely related to the ferroelectric medium. These include the dielectric properties of the film and the coercive electric field that needs to be exceeded for polarization inversion to occur. Therefore, tips with slightly difference shape and size can still write inverted domains with the same size especially at low biases that usually result in small inverted domains. This is the case here in our study.

To illustrate this point, we have characterized the ferroelectric properties of the PZT film used in the 5 km wear test. Figure S7a below shows the capacitance-voltage (C-V) hysteresis

loop in which very good butterfly-like capacitance variation is seen. From this curve we determined that the film has a dielectric constant ε_r = 95.6 and a coercive field E_c = 1.70×10^7 V/m. Given these parameters, we simulated the domain formation in the 50 nm PZT film by an as received PtIr tip (i.e., 20 nm spherical tip) and a worn PtIr tip (i.e., 20 nm cylindrical tip). These are shown in Figures S7b,c below. The white areas correspond to electric field exceeding the experimental coercive field and are a measure of inverted domain volumes. We can see that for a worn tip, its width, i.e., bit size, is only 3 nm larger than the as received (spherical tip), although it penetrates further into the film. Moreover, experimental conditions are usually more complex than the analysis we are showing here in and there are other parameters that influence the bit size such an anti-parallel built-in electric field within the ferroelectric film which is seen in Figure S7a, as well as depolarization field and domain wall forces that all affect the final bit size. In our opinion, this explains why we obtained the same bit sizes before and after the 5 km sliding.

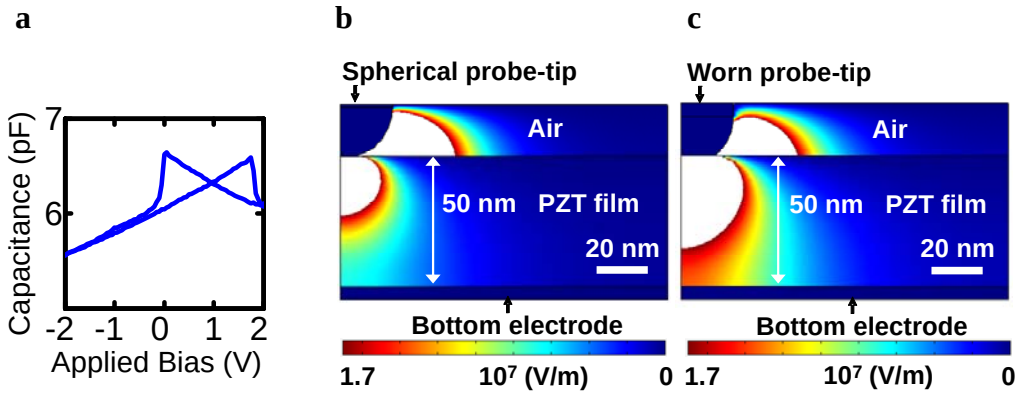

Figure S7. Electric field penetration within PZT film. (a) C-V hysterisis loop of the 50 nm thick PZT film (RMS roughness = 0.17 nm). (b, c) Electric field distributions for a spherical (a) and a worn tip (b).

Carbonaceous contamination from organic films. Wear reduction through conventional lubrication cannot be used in probe-based storage with ferroelectric films as writing media because most common lubricants are organic films, e.g., Z-TETRAOL 2000 (ref. 11 in manuscript). These films induce carbonaceous contamination build-up on the probe-tip during sliding (Figure 25 in ref. 11). Similar results have been observed in the current study prior to PZT-surface cleaning, in which organic-film contaminates are present on the PZT surface. Figure S8 shows images of various probe-tips after 1000 m of sliding. A large amount of carbonaceous contamination is seen.

The build-up on the probe-tips is confirmed to be of carbonaceous nature by performing Energy dispersive X-ray spectroscopy (EDS) on the apex of probe-tips where the contamination was present. Figure S9 shows a typical EDS spectrum where a large carbon peak is clearly detected. Other detected components are Si, O, P and Ir which form the cantilever material and coating.

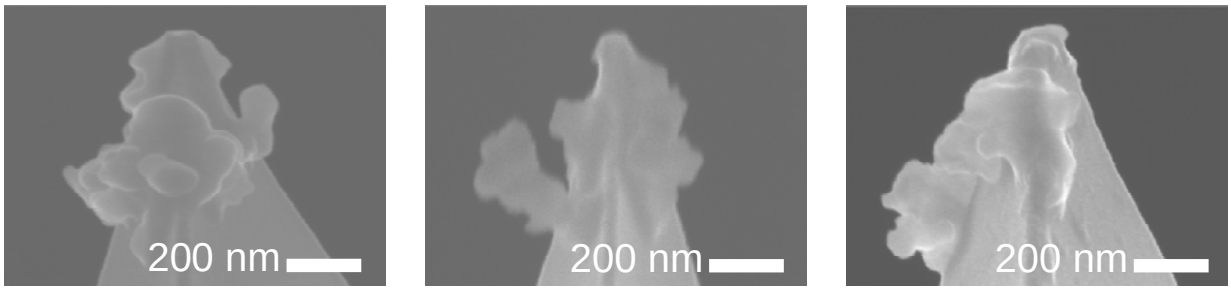

Figure S8. Scanning electron microscope (SEM) images of carbonaceous contamination on PtIr probe-tips after sliding.

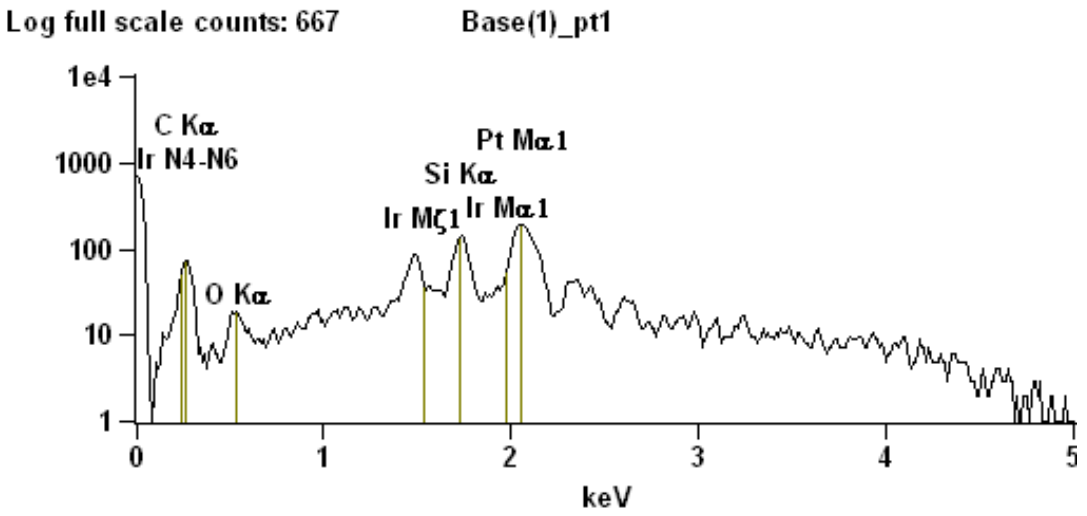

Figure S9. Energy dispersive X-ray spectroscopy **(EDS) spectrum taken on the apex of a probe-tip where contamination build-up was present. C, Si, O, P and Ir components are detected.**

Figure S10a shows PFM height, amplitude and phase images of a 4×4 matrix of inverted domains written by applying 7-10 V (right to left) bias pulses at 100 μs prior to sliding. Inverted domains are clearly seen. However, writing was not possible after sliding except at the highest (10 V) bias pulse (Figure S10b). The pulse writing process was hindered by the carbonaceous build-up which prevents the electric field distribution underneath the probe-tip to penetrate through the PZT film. A high enough voltage has to be applied for that to occur, which is the case of the 10 V bias pulse.

Organic film contaminates were completely removed by cleaning the PZT-surface. The cleaning procedure consisted of sonicating the PZT-samples in acetone (30 minutes), isopropanol (10 minutes), and highly purified water (10 minutes), respectively. This was followed by CO_2 snow cleaning, which consists of flashing the PZT surface with liquid (or gaseous) carbon dioxide. Such flashing is known to remove submicron particulates and hydrocarbon-based

contamination. Finally a 20-minute U-V ozone cleaning was performed. After this cleaning procedure, no carbonaceous build-up was observed before and after sliding. The write and read processes were also not affected.

Note that it was reported in ref. 9 that various organic lubricants were used to reduce wear and no measurable effects on the readback signal were observed. However, the reported scanning distances were very short (no longer than 100 μm). From experiments we performed, at these short distances, the carbonaceous built-up is very small and has no effect on read/write performance. It is only at much longer distances (>100 m) that such a carbonaceous built-up becomes significant to affect read/write operations. As mentioned previously, such a built-up on tips can be seen in Figure 25 of ref. 11 where organic lubricants were used. Note also that at the short distances reported in ref. 9, no noticeable wear can be detected even under dry conditions. However, significant wear has been reported by Bhushan et al. (ref. 11 in the manuscript) even when similar organic lubricants (e.g. Z-TETRAOL) were used over 300 m sliding distances (Figure 25 in ref. 11), which is less than 10% of the demanded sliding distance during the life-time of probe-based storage devices.

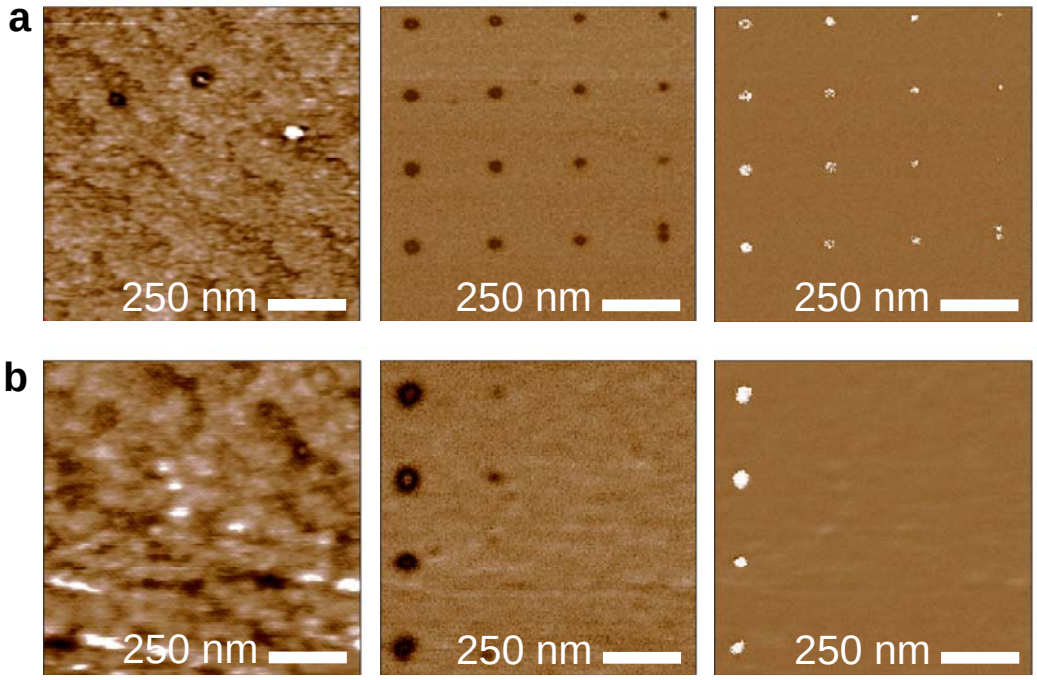

Figure S10. PFM height, amplitude and phase images of a 4×4 matrix of inverted domains written by applying 7-10 V (right to left) bias pulses at 100 µs prior to sliding. (a) Before sliding. (b) After sliding. Only inverted domains obtained at 10 V were observed. Writing at smaller bias pulses was not possible due to the carbonaceous contamination at tip apex.

Effect of roughness on bit size and wear volumes. Figure S11 shows topographic AFM images of four PZT films used possessing an RMS roughness of 0.17, 0.23, 0.31 and 0.57 nm, respectively. The film surfaces were used for the roughness effect study and are statistically equivalent and are characterized by a Gaussian distribution (Figure S11e). Also shown in Figure S11 are SEM images of the PtIr probe-tips after 500 m of sliding under 25% RH (as-received probe-tips with 20 nm radius are always used for each experiment). Figures S12a-c show representative inverted domain dots before and after the 500 m sliding experiments, which depict the extend of dot increase written before and after sliding on the samples with 0.17, 0.31 and

0.57 nm RMS roughness, respectively. Clearly, increasing the RMS roughness increases the wear rate considerably and degrades the write-read resolution. This is further discussed in the main manuscript.

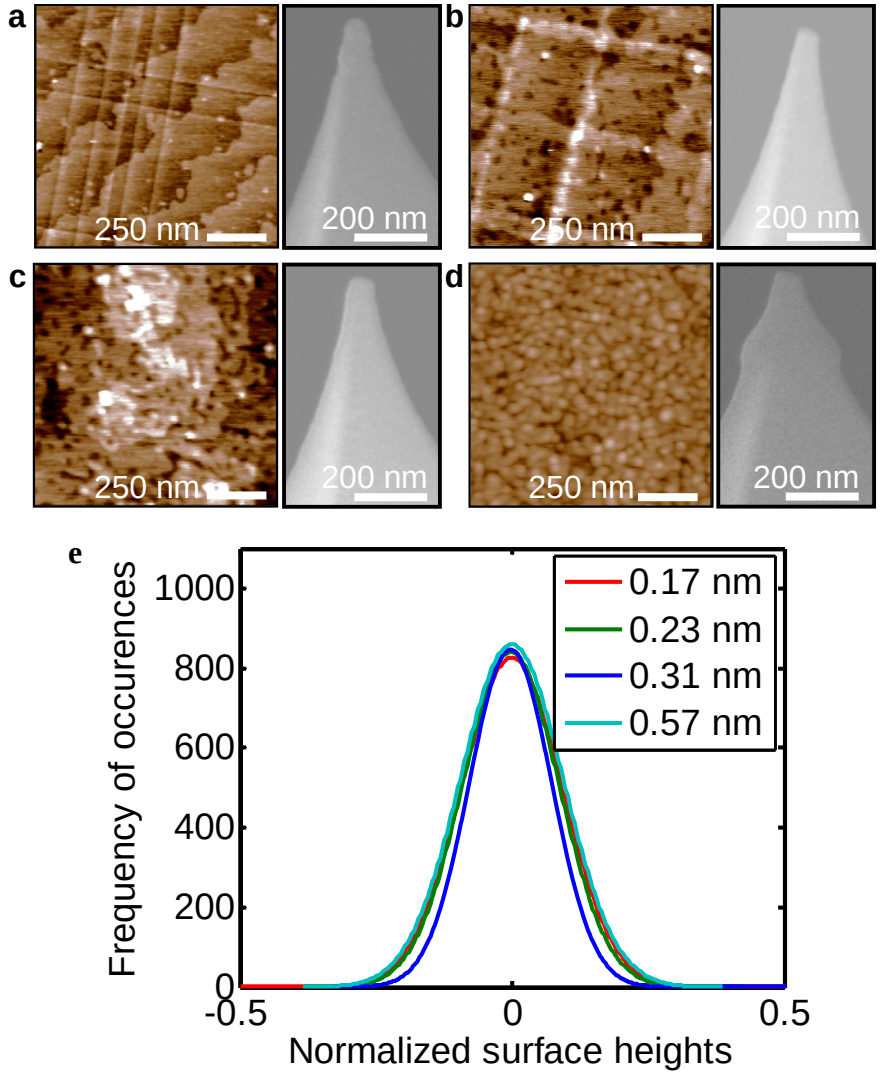

Figure S11. Effect of roughness on bit size and wear volumes. (a-d) Left: topographical height images of PZT films with 0.17 nm (a), 0.23 nm (b), 0.31 nm (c) and 0.57 (d) RMS roughness, respectively. Right: SEM images of PtIr tips after 500 m sliding over the various PZT-films at 5 mm/s with an applied normal force F_N = 100 nN that is modulated at 200 kHz. (e) Surface roughness measurements on the four PZT samples. The surfaces are statistically equivalent and are represented by a Gaussian distribution.

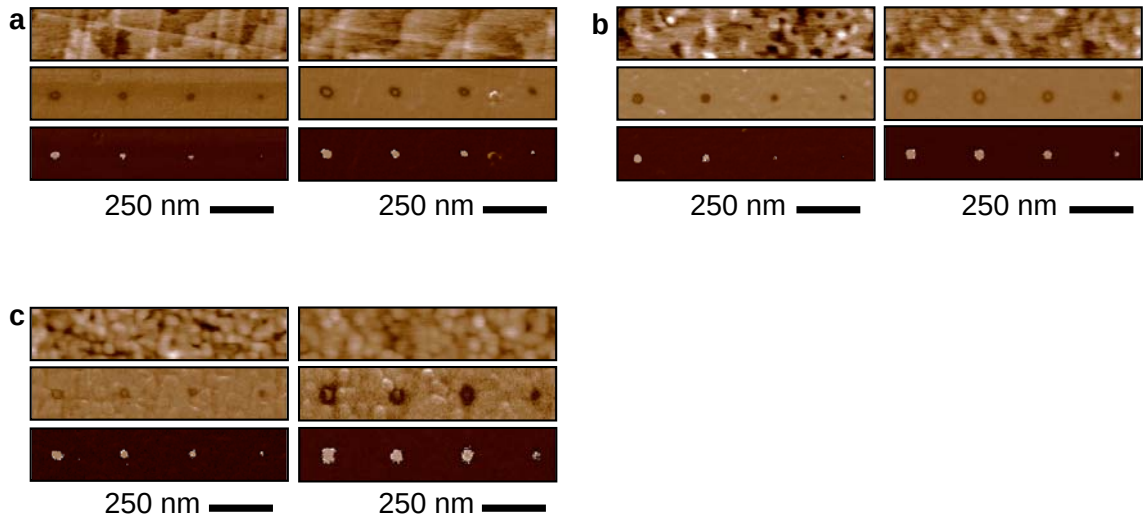

Figure S12. Effect of roughness on bit size increase. PZT films with 0.17, 0.23, 0.31 and 0.57 nm RMS were used. Sliding was performed at 5 mm/s with an applied normal force F_N = 100 nN that was modulated at 200 kHz under 25% RH. (a-c) Representative height (top), amplitude (middle) and phase (bottom) images of inverted domain dots before (left) and after (right) the 500 m sliding experiments. These images depict the dot size increase after sliding on the samples with 0.17, 0.31 and 0.57 nm RMS roughness, respectively. 5-8 V pulses were applied in (a) and 3-6 V pulses were applied in (b), (c). The pulse potential decreases by a 1 V increment (left to right).

Effect of relative humidity on bit size and wear volumes. Figures S13a-c show representative inverted domain dots before and after the 500 m sliding experiments, which depict the dot size increase written before and after sliding at 0%, 25% and 40% relative humidity, respectively. All sliding experiments were performed on the PZT sample with 0.23 RMS roughness (Figure S11b). Bit size and wear volume first decrease after sliding as the RH level is increased from the

dry condition. However, as the RH level further increases, the bit size and wear volume start increasing considerably. This is further discussed in the main manuscript.

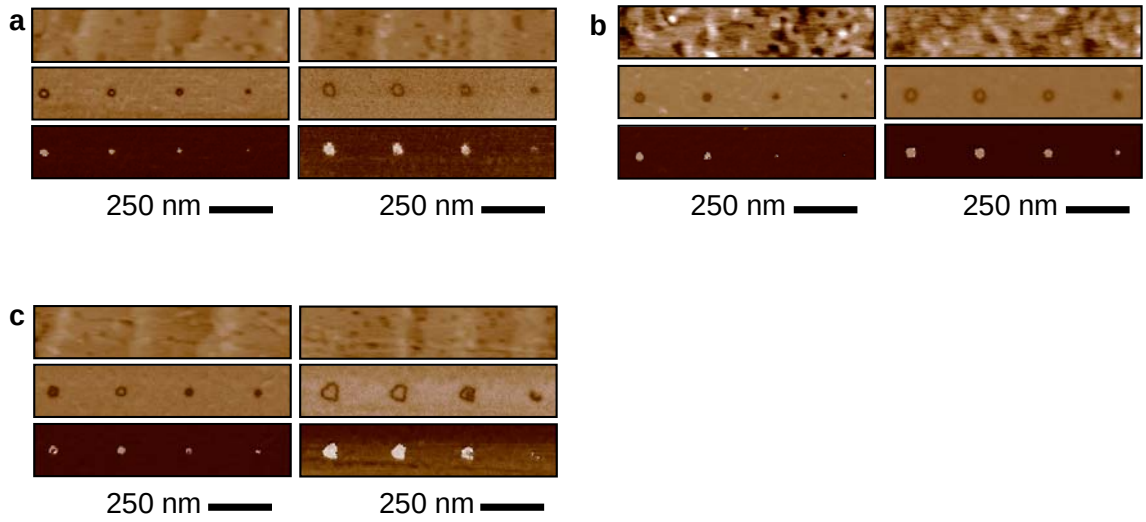

Figure S13. Effect of relative humidity on bit size and wear volumes. (a-c) Representative height (top), amplitude (middle) and phase (bottom) images of inverted domain dots before (left) and after (right) the 500 m sliding experiments. These images depict the dot size increase after sliding on the PZT sample with 0.23 nm RMS roughness under 0%, 25% and 40% RH conditions, respectively. 5-8 V pulses were applied. The pulse potential decreases by a 1 V increment (left to right).